



# Grav3CH\_inv: A GUI-based MATLAB code for estimating the 3-D basement depth structure of sedimentary basins with vertical and horizontal density variation

Erdinc Oksum <sup>1,\*</sup>

*Department of Geophysical Engineering, Suleyman Demirel University, 32200, Isparta, Turkey*



## ARTICLE INFO

**Keywords:**  
Sedimentary basin  
Gravity anomaly  
Basement depth  
Modelling  
MATLAB

## ABSTRACT

This study presents a software tool Grav3CH\_inv developed to estimate the three-dimensional depth structure of sedimentary basins from their gravity data through an iterative process. The algorithm linked to the developed code operates recursively both in the wavenumber domain and in the space domain based on a triple method combination. The modelling strategy allows considerations of the model space with an exponential increase in density with depth and also with density variations in the horizontal direction. The accuracy of computation of gravity anomalies in the FFT-based forward procedure is also increased by using the shift-sampling technique which minimizes discretization effects during transformations between the space and wavenumber domains. Given the observed gravity anomalies and the density design of the basin, the iterative procedure performs automatically until the goodness of the fit between the observed and modeled anomaly, either the root-mean-square error or the largest error is below its pre-assigned value. As an advantage, the computing time is acceptably short for such a kind of an modelling problem. The GUI-enabled interactive control functions of the Grav3CH\_inv code allow users to set optional settings, style of outputs and export formats, and facilitate operations without requiring coding expertise to perform the relevant procedures of the algorithm. The feasibility and accuracy of the proposed software is demonstrated by evaluating the synthetically produced gravity anomalies of various 3D basin models and also by analyzing an actual gravity data from the Los Angeles basin, California.

## 1. Introduction

Investigations on sedimentary basins are generally associated with their development and economic significance. Economically, sedimentary basins are the most important sources of energy-related products such as oil, gas, coal, uranium and geothermal fluids, and the largest deposit reservoirs for many minerals. Determining the presence and spatial position of smooth depressions and uplifts in the basement relief of a sedimentary basin may be guiding in locating stratigraphic and structural oil traps (Chakravarthi et al., 2007; Silva et al., 2010). Besides, basement relief estimates can also provide important contributions in understanding aquifer structures in hydrogeological studies (Bohidar et al., 2001; Himi et al., 2017; Lekula et al., 2018), and in understanding the flow rate of the discharge in glaciological investigations (Venteris and Miller, 1993), or can have important implication as a density determination tool in landslide studies (Mantlik et al., 2009).

The gravity method is an effective way to approximate the depth structure of a sedimentary basin because variations in gravity can be observable due to the presence of substantial contrast in density between the sedimentary infill and the mass below the basement interface (Silva et al., 2006; Chakravarthi and Ramamma, 2015). The commonly used mathematical geometries in sedimentary basin modelling are the polygonal model (Talwani et al., 1959) or the stacked prism model (Bott, 1960). A number of algorithms available apply a uniform density in their inversion schemes for the units above the basement interface (Cordell and Henderson, 1968; Murthy and Rao, 1989; Barbosa et al., 1997, 1999; Mendonca, 2004; Pallero et al., 2015, 2017; Ekinci et al., 2021). However, for the thick basins, the density of sedimentary rocks varies with depth, so this assumption is often unrealistic (Chakravarthi et al., 2013, 2017; Mallesh et al., 2019; Florio, 2020). Several studies have shown that the densities of the sedimentary fills generally increase with depths due to increasing pressure (Athy, 1930; Hedberg, 1936; Hughes

\* Corresponding author.

E-mail address: [erdincoksum@sdu.edu.tr](mailto:erdincoksum@sdu.edu.tr).

<sup>1</sup> Erdinc Oksum contributed to the development of the code given with the proposed algorithm and the writing of the article and its scientific content.

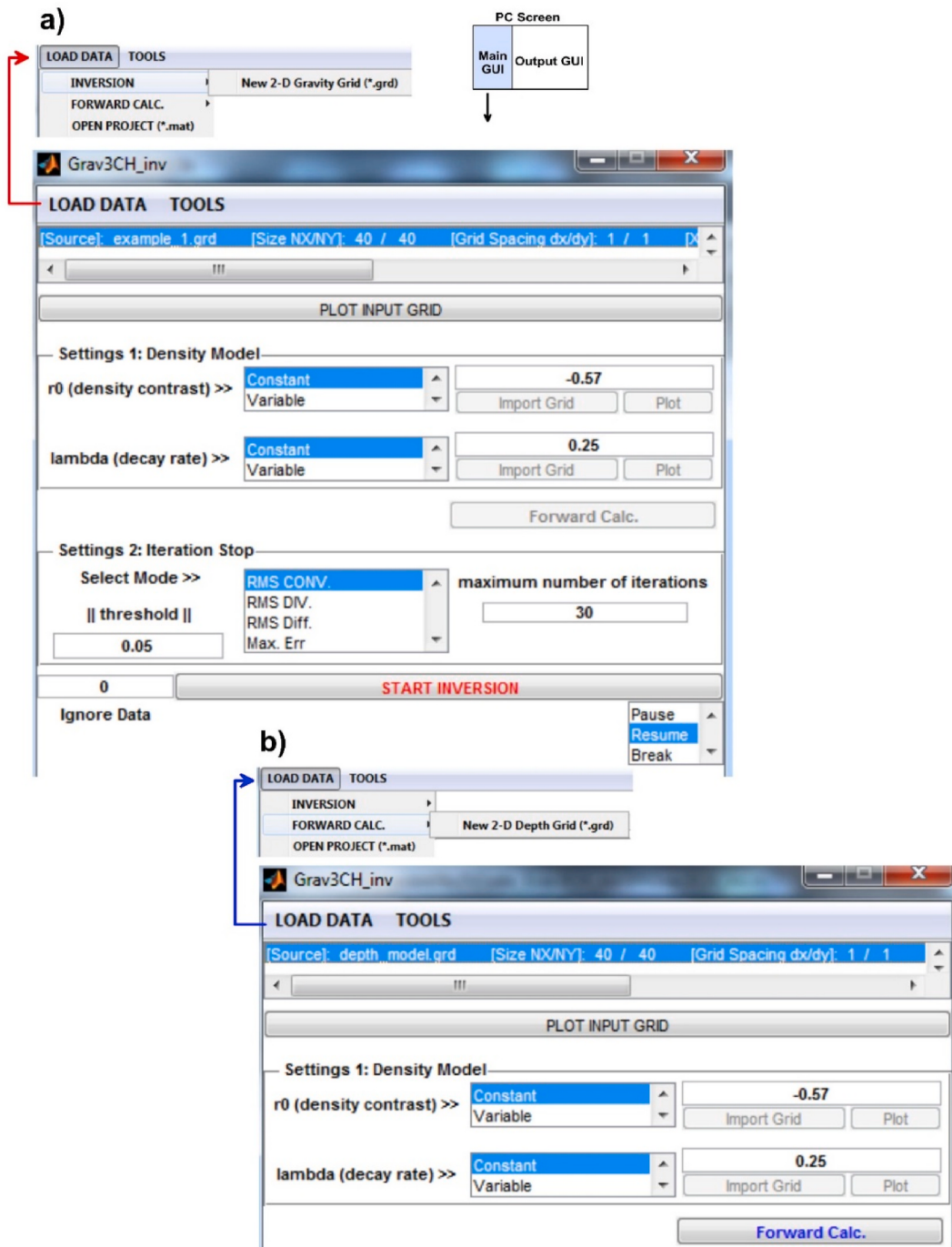


**Fig. 1.** Screen shot of Grav3CH\_inv Gui after a successful data loading, (a) inversion mode, (b) forward calculation mode.

and Cooke, 1953; Cordell, 1973; Crosby et al., 2006; Tenzer and Gladikh, 2014; Cai and Zhdanov, 2015). Therefore, the practical benefits of algorithms considering constant density for the interpretation would be insufficient, particularly when the densities in the mass above the interface are non-uniform with depth. Hence, other methods that incorporate varying density models with depth for more accurate modellings have been proposed, for example, the linear density function (Murthy and Rao, 1979), the quadratic density depth relation (Bhaskara Rao, 1986; Feng et al., 2016), the hyperbolic law (Litinsky, 1989), the cubic function (Garcia-Abdeslem, 2005), the parabolic density depth relation (Chakravarthi et al., 2002; Chakravarthi and Sundararajan, 2004; Silva and Santos, 2017) and the exponential density function (Granser, 1987).

In general, the sediment density increases rapidly at shallow depths and progressively less rapidly towards deeper. Although each density function has its own benefit for a reliable interpretation, density information from wells, lithological records, and sample density measurements are always needed to define an appropriate function that could give the most effective solution. The density-depth dependency of a sedimentary basin may often be simulated by an exponential relation for the case the high contrast in density exists at the shallower depths, while the density contrast attains its minimum at the lower stratigraphic unit of a thick sedimentary sequence (Athy, 1930; Cordell, 1973; Maxant, 1980; Garcia-Abdeslem, 1992; Chappell and Kusznir, 2008; Chakravarthi et al., 2013; Gu et al., 2014; Mallesh et al., 2019). If the appropriate function is exponential, it is not possible to derive an analytical

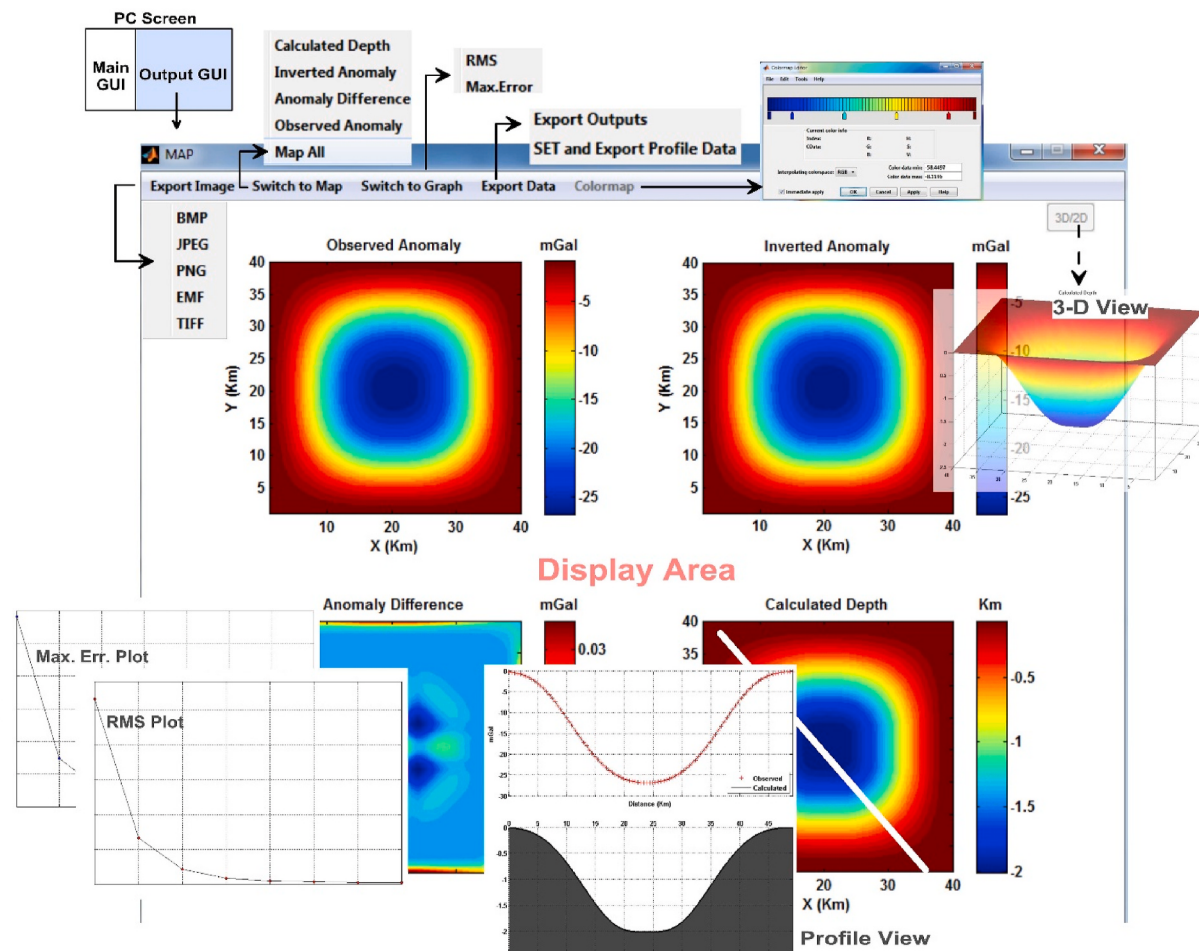


**Fig. 2.** Illustration of representative output plots from Grav3CH\_inv Gui after a successful interpretation.

expression in the space domain for the gravity effect of anomalous sources (Chai and Hinze 1988; Chakravarthi, 2009). To achieve this, a number of frequency domain algorithms have been developed to simulate the gravity effect of source bodies varying in density exponentially with depth. For instance, Cordell (1973) divided the model space of a profile section into prismatic compartments and presented an iterative routine which incorporated both the gravity effect and its vertical gradient. Granser (1987) developed a frequency-domain algorithm based on Parker's (1973) method for calculations of the model gravity anomalies of structures including exponential change in density with depth. Later, Chai and Hinze (1988) derived a forward formula for a 3D vertical rectangular prism realized in the wavenumber domain in which an exponential change in density contrast was considered, followed by a shift-sampling technique to improve the precision of transformation from the wave number domain to the space domain. In another attempt by Bhaskara Rao et al. (1993), graphical methods deduced from characteristic values of frequency-domain transforms derived for a number of simple shaped bodies with exponential density contrast were used for the analysis of the gravity anomalies of sedimentary basins. Feng et al. (2014) extended the Parker-Oldenburg algorithm for a 3D case and introduced a gravity data inversion compatible with lateral and vertical density consideration.

It is evident that frequency domain techniques in calculating gravity anomalies are faster than space domain techniques, thus, FFT-based methods result in computer time-efficient practical applications (Granser, 1987). On the other hand, the utility of many methods depends on the precision of the transformations between the space and wavenumber domains (Chai and Hinze, 1988). Several researchers have built computer programs based on FFT algorithms, including inversion

schemes to reconstruct the density interface geometry from the gravity data. Although those based on Parker (1973) and Oldenburg (1974) have a short estimation time and are capable for large data sets (Nagendra et al., 1996; Gomez-Ortiz and Agarwal, 2005; Shin et al., 2006), a fixed datum plane and/or filtering of the data is required for their procedural convergence of inversion. Another computer program for the gravity modelling of sedimentary basins by Pham et al. (2018) performs a recursive procedure by computing gravity anomalies using the forward algorithm of Granser (1987) and modifying the depth estimates in the spatial domain using the modelling scheme of Cordell and Henderson (1968). Although their algorithm by this combination does not require filtering and the average depth plane of the interface, the density-depth dependence of the model space is limited to the assumption that it varies only in the vertical direction.

In this paper, it is aimed at presenting an alternative software tool for simulating the 3D depth structure of a sedimentary basin from its gravity field. The proposed algorithm is based on utilizing the inverted Bouguer slab relation of Cordell (1973) in a recursive procedure which combines both the frequency domain method of Chai and Hinze (1988) and the space domain technique of Cordell and Henderson (1968). By this combination, the modelling scheme is capable to allow considerations of the density variety of the model space both in the vertical and horizontal directions simultaneously. The precision of the transformations between the space and wavenumber domains during computation of gravity anomalies is also improved by adopting the shift-sampling method suggested by Chai and Hinze (1988). The presented algorithm linked to the code Grav3CH\_inv.m is built in MATLAB (R2013b) with a graphical interface which guides the user to manage the operation simply without any requirement of coding experience. The software is tested for its

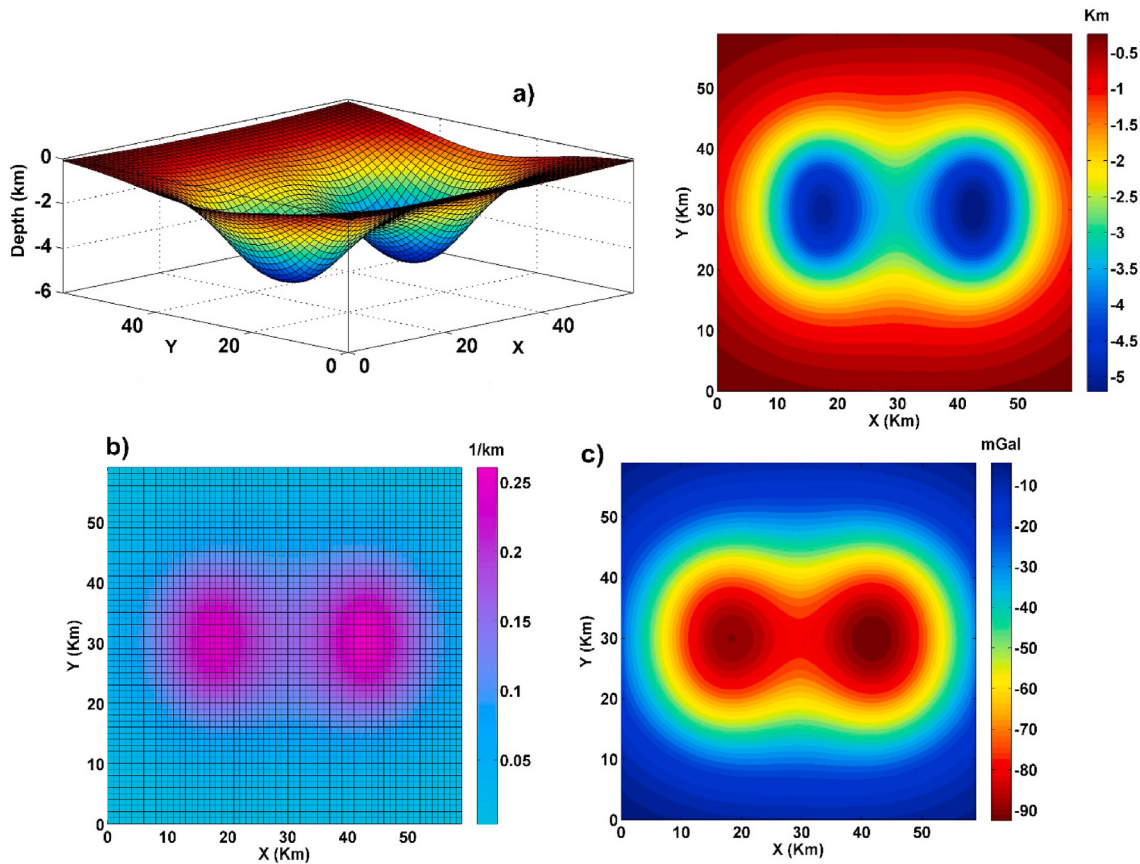


**Fig. 3.** Synthetic example Model-1 considering vertical and horizontal density variation, (a) the 3D view and the plan view of the of the simulated basin model used for producing the synthetic data, (b) the horizontal variation of the decay constant ( $\lambda(x,y)$ ) (c) the theoretical gravity anomaly of the basin produced using Eq. (4) with density model according to the equation  $\rho(x,y,z) = -0.6e^{-\lambda(x,y)z}$ .

practical application and accuracy on both synthetic and actual gravity data.

## 2. Theory

Defining the model space by a three-dimensional Cartesian coordinate system where its pair-wise perpendicular axes are  $x$ ,  $y$  and  $z$  pointing eastwards, northwards and vertically positive downwards, respectively, and the sediment's density contrast at any location  $(x, y, z)$  is simulated by an exponential decrease with depth using the function (Granser, 1987; Cordell, 1973):

$$\rho(x, y, z) = \rho_0 e^{-\lambda(x, y)z} \quad (1)$$

where  $\Delta\rho_0$  is the surface density contrast, and  $\lambda(x, y)$  is the decrement of contrast with depth, the gravity anomalies originating from the sedimentary basin by means of a series of prisms can be simulated from the Chai and Hinze (1988) method,

$$\Delta g = \sum_{i=1}^m \sum_{j=1}^n \Delta g_{ij} \quad (2)$$

where  $m$  and  $n$  are the grid size in the north and east, respectively. Here,  $\Delta g_{ij}$  is the gravity anomaly due to a vertical rectangular prism  $(i, j)$

whose top is located at zero (km) and bottom is located at  $z$  (km), its center coordinate is  $(\alpha_i \beta_j)$ , half widths along the east and north directions are  $2a$  and  $2b$ , respectively.  $\Delta g_{ij}$  is given by Chai and Hinze (1988):

where  $\gamma$  denotes the gravitational constant,  $F^{-1}[\cdot]$  is the inverse Fourier transform, and  $s = \sqrt{u^2 + v^2}$  where  $u$  and  $v$  are the wavenumber coordinates. The transformation of the anomaly spectrum back to the final product of the space domain is typically based on the standard FFT algorithm where the precision of this transformation depends on data spacing. Theoretically, by increasing the number of the data points and area of the data set, the accuracy of the transformation between the wavenumber domain and the space domain can be improved. Chai and Hinze (1988) suggested the use of the shift sampling technique to increase the precision of the inverse numerical Fourier transform based on the discrete Fourier transform deviation equation. Hence, Eq. (3) becomes:

$$\Delta g_s = F^{-1} \left[ 2\pi G \Delta \rho_0 4ab \operatorname{sinc}(2ua) \operatorname{sinc}(2vb) \times \sum_{i=1}^m \right. \\ \left. \times \sum_{j=1}^n \frac{1}{\lambda_{ij} + 2\pi s} \{1 - e^{-(\lambda_{ij} + 2\pi s)z_{ij}}\} e^{-2\pi i(u_s \alpha_i + v_s \beta_j)} \right] \quad (4)$$

$$\Delta g_{ij} = F^{-1} \left[ 2\pi G \Delta \rho_0 4ab \operatorname{sinc}(2ua) \operatorname{sinc}(2vb) \times \frac{1}{\lambda_{ij} + 2\pi s} \{1 - e^{-(\lambda_{ij} + 2\pi s)z_{ij}}\} e^{-2\pi i(u_s \alpha_i + v_s \beta_j)} \right] \quad (3)$$

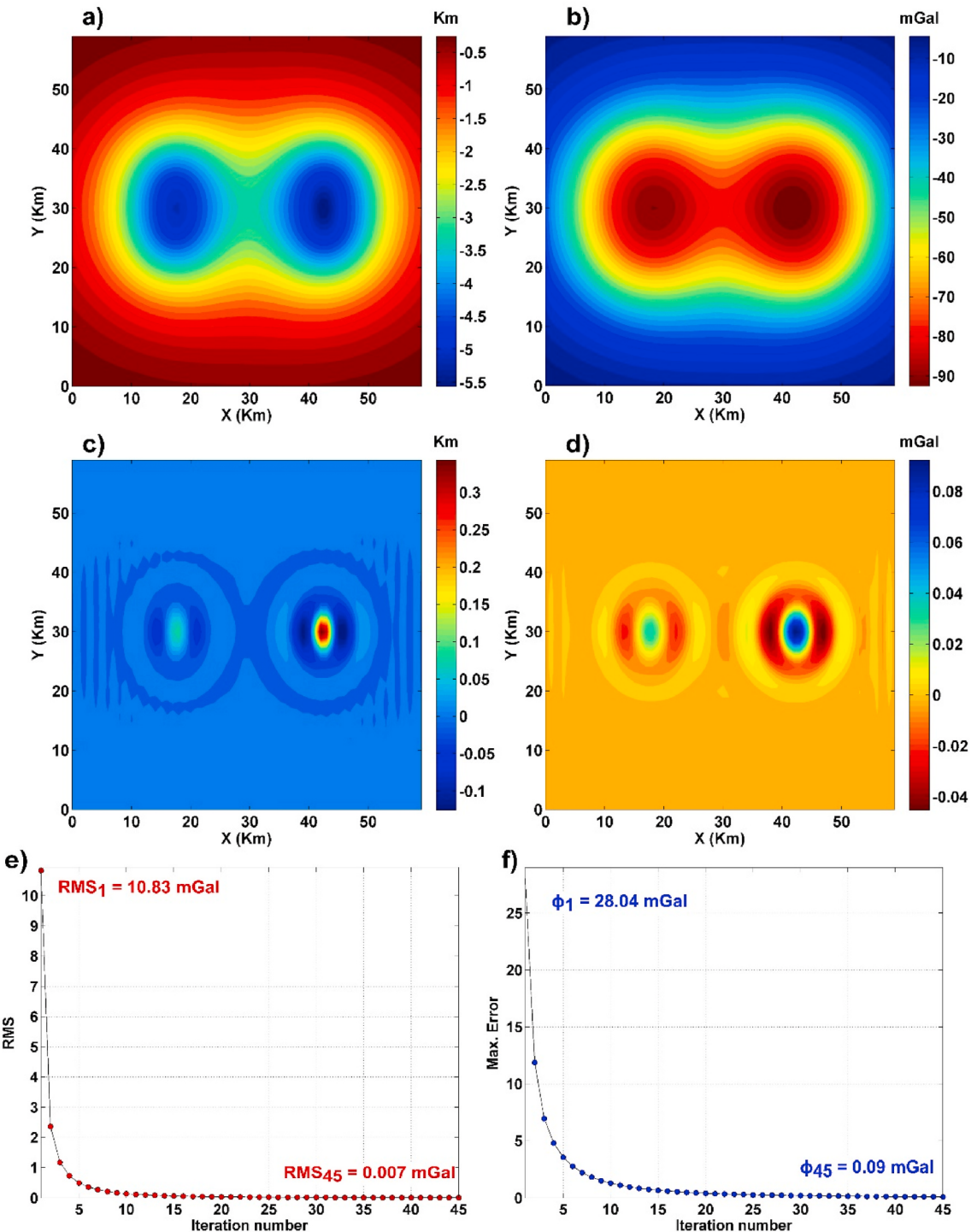


**Fig. 4.** Modelling results of basin Model-1, (a) inverted depths, (b) calculated gravity anomaly from the inverted depth, (c) the difference between the actual and inverted depth, (d) the difference between observed and computed gravity anomaly, (e) variation of RMS error versus iteration number, (f) variation of the largest error  $\varphi$  versus iteration number.

where  $u_s = u + \text{shiffu}$ ,  $v_s = v + \text{shiffv}$ , and  $s_s = \sqrt{u_s^2 + v_s^2}$ . Here, the optimum shift parameter for minimizing the discretization effect is  $\text{shiffu} = \text{shiffv} = 0.26$  for 2-D transforms (Chai and Hinze, 1988). Then, using the shift-sampling technique,  $\Delta g_s$  is calculated and multiplied by  $e^{2\pi\sqrt{-1}\left(\frac{(i-1)\text{shiffv}}{m} + \frac{(j-1)\text{shiffu}}{n}\right)}$ . Its real part is the result. From Eq. (4), it is noted that the algorithm is valid to consider also horizontal density variation in the model space because the  $\lambda$  parameter of prism models is allowed to vary.

Chai and Hinze (1988) combined the forward formula in the wave-number domain and Bott (1960) technique in the space domain for mapping the basement interface. Here, another combination is introduced that is based on Equation (4), the initial depth approximation of Cordell (1973) and the recursive depth improvement of Cordell and Henderson (1968). The procedure begins by estimating an initial depth model  $z(x, y)$  of the basement structure. Following Cordell (1973), the initial model of the basement with exponential density contrast variation can be estimated as:

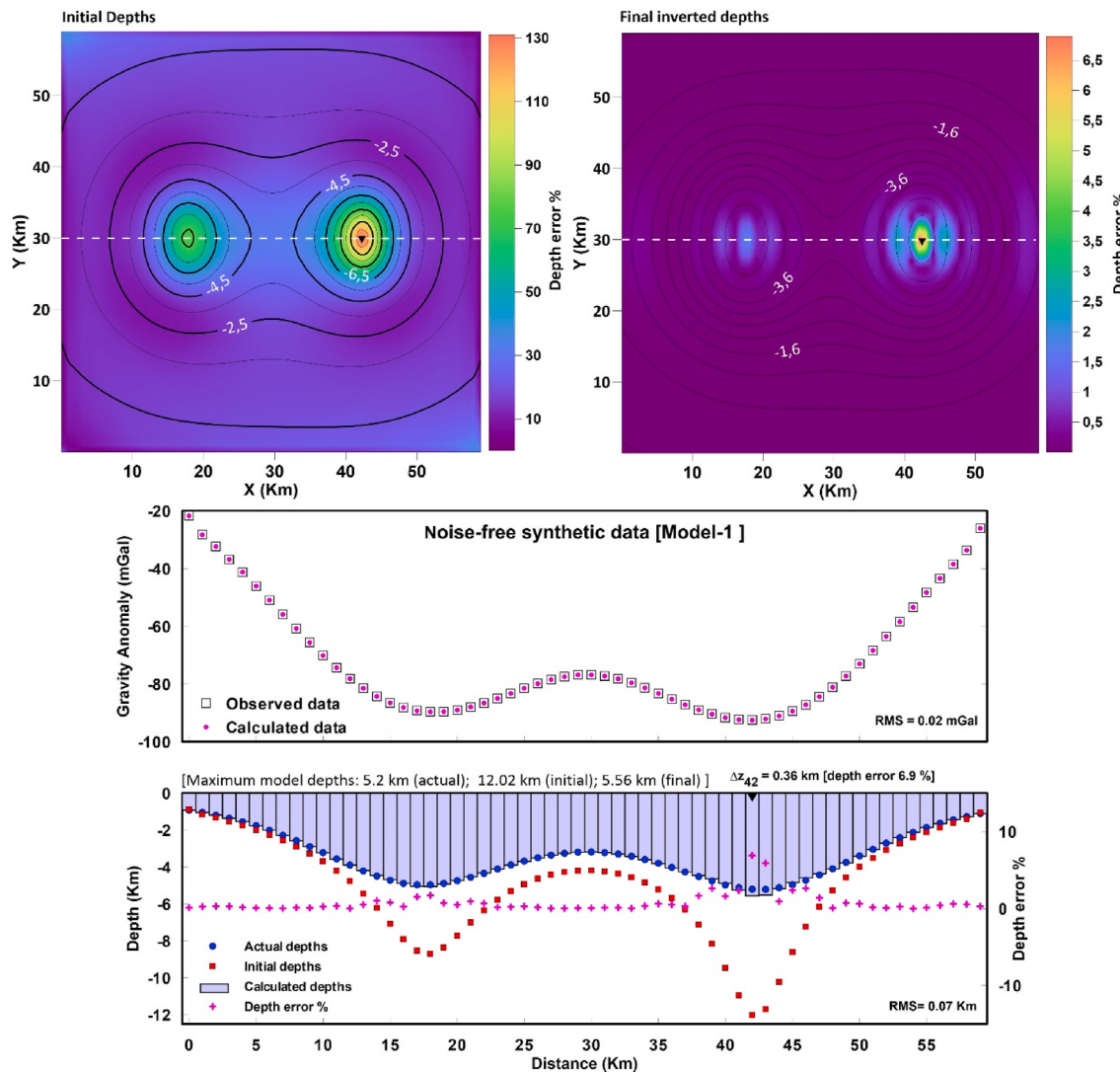


**Fig. 5.** Contour plots of the initial and the final inverted depths of the algorithm calculated from the synthetic data of Model-1 and their percentage errors according to the actual model depths (upper panel), and the results along a profile through the deepest point of the model in comparison with the actual data (lower panel). The white lines on the maps show the location of the profile data presented in the lower panel. The triangle symbol denotes the horizontal location of the deepest point of the actual depth model.

$$z_{(i,j)}^{(1)} = -\frac{1}{\lambda_{(i,j)}} \ln \left( 1 - \frac{\lambda_{(i,j)} g_{obs(i,j)}}{2\pi\gamma\rho_0} \right) \quad (5)$$

where,  $g_{obs(i,j)}$  is the observed gravity at mesh point  $(i, j)$ . Then, using the initial depth model from Eq. (5), the model gravity anomalies  $g_{calc(i,j)}$  are calculated for each observation point using Eq. (4). Cordell and Henderson (1968) proposed estimating the next model improvement by the following relationship:

$$z_{(i,j)}^{(t+1)} = \frac{g_{obs(i,j)} - g_{calc(i,j)}^{(t)}}{g_{calc(i,j)}^{(t)}} z_{(i,j)}^{(t)} \quad (6)$$

where  $t$  is the number of the iteration steps. Following this, the ratio given above is used to modify the bottom depths of prisms instead of using again an infinite-slab estimate as in the Bott (1960) technique. The iterative method efforts to minimize the difference in all observations between the observed anomaly and the calculated one. Thus, after each iteration, the computation of the gravity anomaly due to the updated depth model continues until a desired fit to the observed anomaly is achieved where the root mean square error (RMS) may be the quantity of this goodness,

$$RMS_i = \sqrt{\frac{\sum_{i=1}^m \sum_{j=1}^n (g_{obs(i,j)} - g_{calc(i,j)})^2}{m \times n}} \quad (7)$$

$$\text{or the supremum (sup) of the anomalies difference (largest error) } \varphi, \\ \varphi_i = \sup \{ |g_{obs(i,j)} - g_{calc(i,j)}| \}: \text{ for all } i, j. \quad (8)$$

as a better measure in the case of occurrence of a large variation in the derived model of the course of RMS (Cordell and Henderson, 1968).

### 3. Description of the Grav3CH\_inv GUI

The Grav3CH\_inv code is supported by a practical user interface that includes interactive control functions which make it easy for the user to configure the settings prior the modelling as well as setting the optional display or export formats of the outputs. When the program is first run, it pops up the main graphical interface covering a quarter of the screen on the left side. The remaining part of the screen is reserved for a second GUI which pops up after a successful inverting enabling the control of display and storing of outputs. Fig. 1 illustrates the configuration of the main GUI.

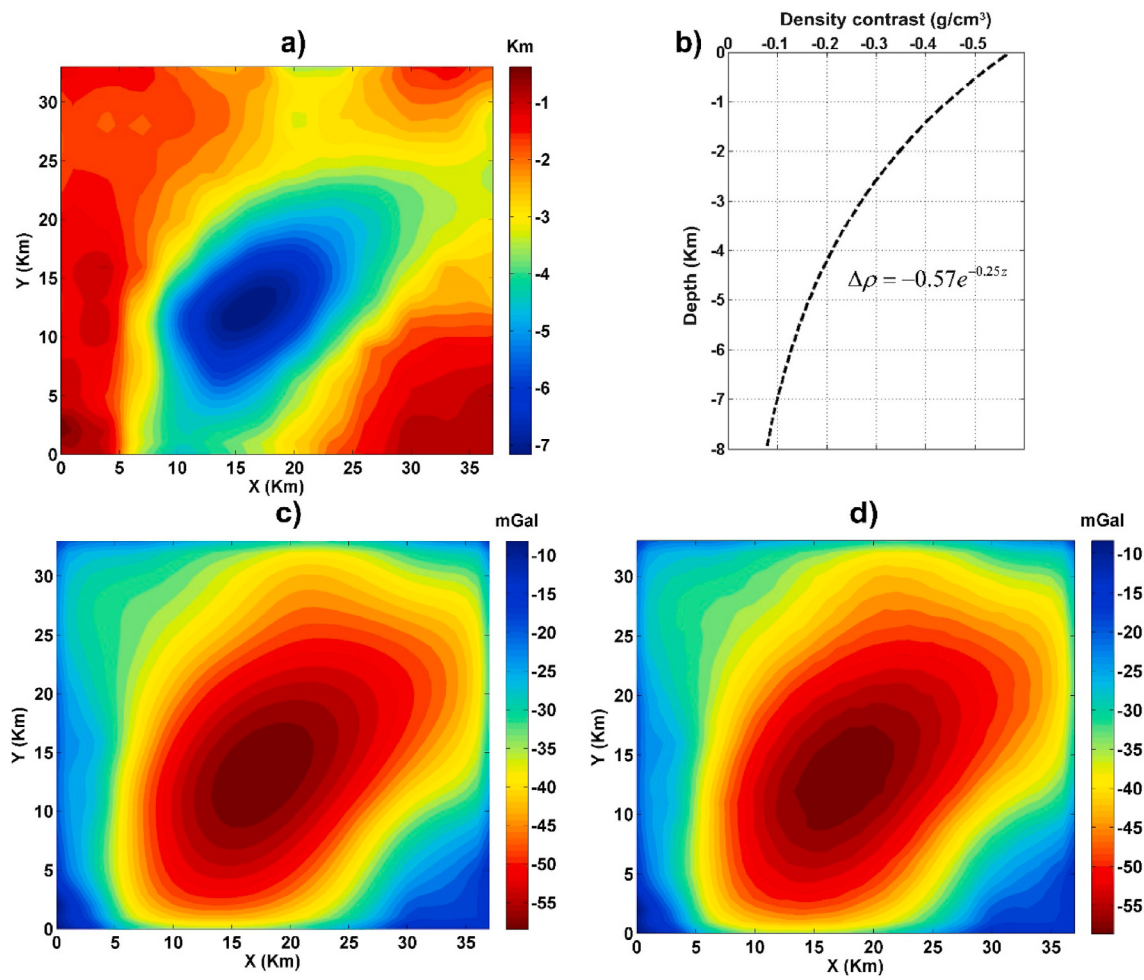


**Fig. 6.** Synthetic example Model-2 considering vertically density variation, (a) the plan view of the of the simulated basin model used for the producing synthetic data, (b) the density contrast of sediments within the basin model vary according to the equation  $\Delta\rho = -0.57e^{-0.25z}$ , (c) the theoretical noise-free gravity anomaly of the basin produced using Eq. (4), (d) the noise-corrupted gravity anomaly.

By the main GUI, the user can operate either for the gravity modelling scheme (Fig. 1a) or for generating computed gravity anomalies of a certain depth model (Fig. 1b) which might be used for the removal of regional effects of deep layers as a prior process of inversion. It includes menu items: for loading gridded gravity (or depth) data for a modelling (or a forward) procedure; editable cells and optional boxes for the configuration of the density model and the iteration stop criterion, and confirmation buttons that initiates the intended operation. There is also an additional toolbox available for performing an exponential fit to a given measured density-depth information. In the inversion mode, the interactive [Load Data-New 2D Gravity Grid] menu at the top on the left of the main GUI (Fig. 1a) is used to import the gridded gravity data set which supports the common grid formats of the Surfer program (Golden Software). The mesh grid intervals to the east and north are required to be equal and any blank in input is not allowed. The mesh details of the enabled input data will be described in the topmost info box after complete data loading, and a color-filled contour map will be displayed. Next, the set of the density model is required in the panel “Settings-1”. Here, while considering that the density contrast varies only vertically, a single value is asked for the rate of decay factor. However, considering with the case of a laterally varying rate of decay factor and/or a laterally varying surface density, 2-D grid inputs are required. The distances of the map units are expressed in km, the gravity in mGal and the unit of densities are in g/cm<sup>3</sup>. Optionally, some data from the edges of the model space can be omitted by editing the “Ignore Data” cell (default is zero) to avoid edge effects. In this case, the RMS or the greatest error calculation is made by omitting these specified amounts of data close to the edges.

However, an alternative reasonable solution would be to use a wider window of input data. The stopping criterion of the iteration procedure can be set in the panel “Settings-2” by enabling the list box for the desired criterion. Here, the interactive list box enables the user four different modes as stopping criteria: the RMS-CONV (RMS convergence-mode), RMS-DIV (RMS divergence-mode), RMS-Diff (RMS difference-mode) and the Max Err. (greatest error-mode). In the RMS convergence or the greatest error modes, the iteration stops when the measure of the fit falls below its predefined threshold, while in the RMS difference-mode, it stops when the difference between the RMS values from successive steps is below the given threshold. In the RMS divergence-mode, the iterative procedure terminates when the RMS exceeds its previous value. For all the options, the procedure stops when it completes the predetermined number of iterations limit. In addition to these automatic stopping criteria, the GUI interface of the code also allows the user to pause the procedure in order to instantly see the results of any iteration stage and allow the procedure to resume or stop where it left off. All entries are memorized by the code into a temporal file connected to the input grid which can be recalled optionally to be stored together with the results after a final approval by the user.

After validating the entries, the process starts with building the initial depth estimates from the inverted Bouguer slab relation compatible with the use of exponential density contrast variation by Eq. (5) and continues to operate a loop between the frequency domain and the space domain for calculation of the gravities by Eq. (4) and improvement of their inverts by Eq. (6) until the matching criterion between the actual and calculated gravity anomalies is achieved. The measures of the fit after each iteration

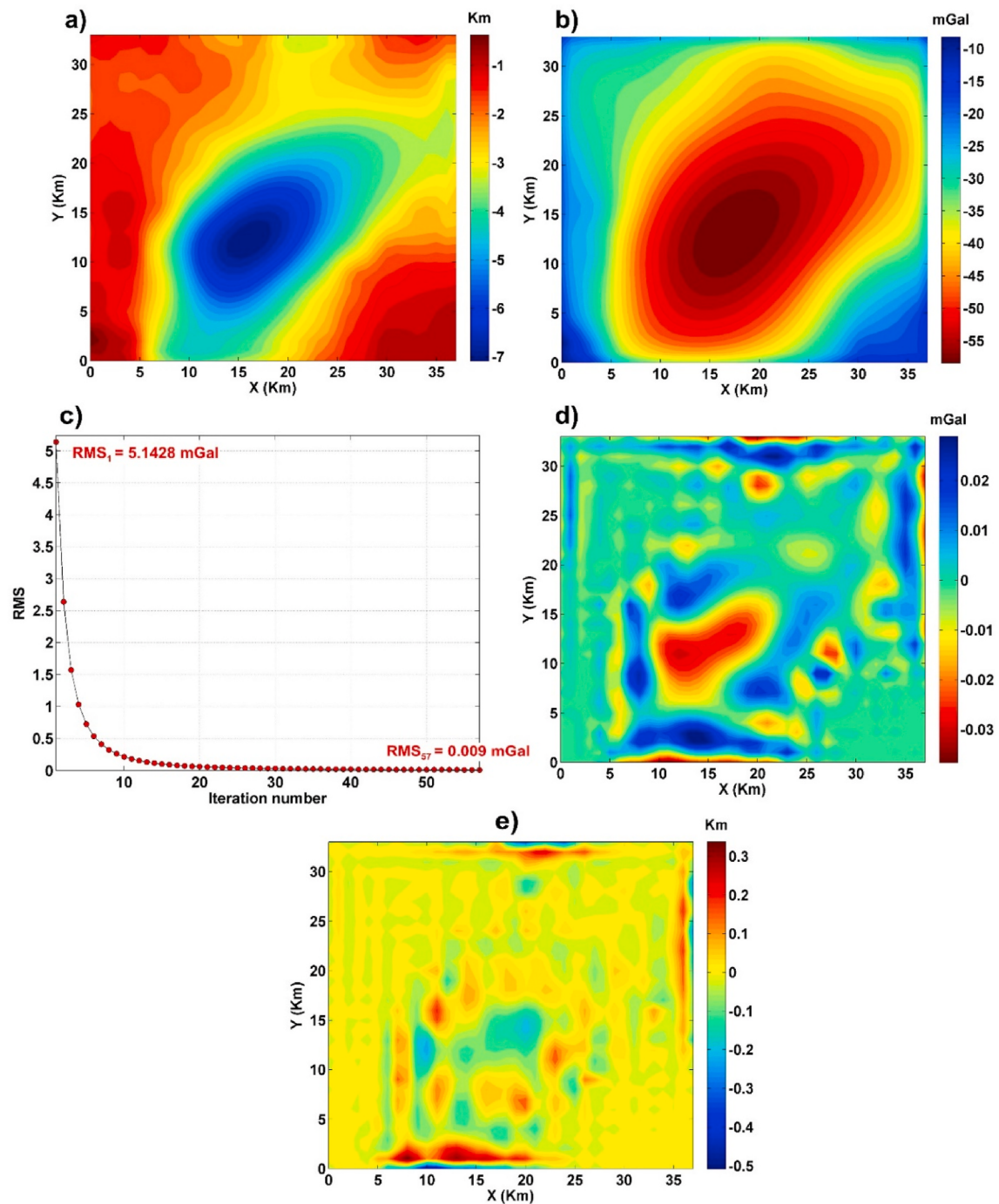


**Fig. 7.** Modelling results of Model-2 in noise-free case, (a) inverted depths, (b) calculated gravity anomaly from the inverted depths, (c) variation of RMS error versus iteration number, (d) the difference between observed and computed gravity anomaly, e) the difference between the actual and inverted depths.

are instantly displayed on the main GUI. Finally, the code records the gravity response and the inverted basement depth obtained at the stopping step of the iteration, the residual between the actual and modeled gravity anomalies and the values of fits after each iteration to the associated temporal file. Afterwards, a second user interface emerges and enables the user to display and export any of the produced maps or graphics in optional preferences, for example map displays in 2D or 3D, color adjustment, view of results at any profile section and exporting to numeric or image formats (Fig. 2). Exporting can be done as an image for a selected output or numerically for all outputs to a user-defined folder. In case of all selected, the defined file name is common for all outputs while the code automatically adds an informative extension of the available output. Formats for

numeric exports (\*.grd, \*.dat) are compatible with the formats of Golden Software, whereas the image exports are supplied in some commonly used graphic formats (\*.bmp, \*.jpeg, \*.png, \*.emf, \*.tiff) of 300 dpi in resolution. All the output data together with the settings are also stored as a binary MATLAB file (\*.mat) where this can be imported by the code at any time for a review or an update of the modelling.

#### 4. Synthetic data application

In this part, the applicability and effectiveness of the algorithm are shown by modelling of synthetically generated gravity datasets of simulated 3D sedimentary basin models with density contrasts varying

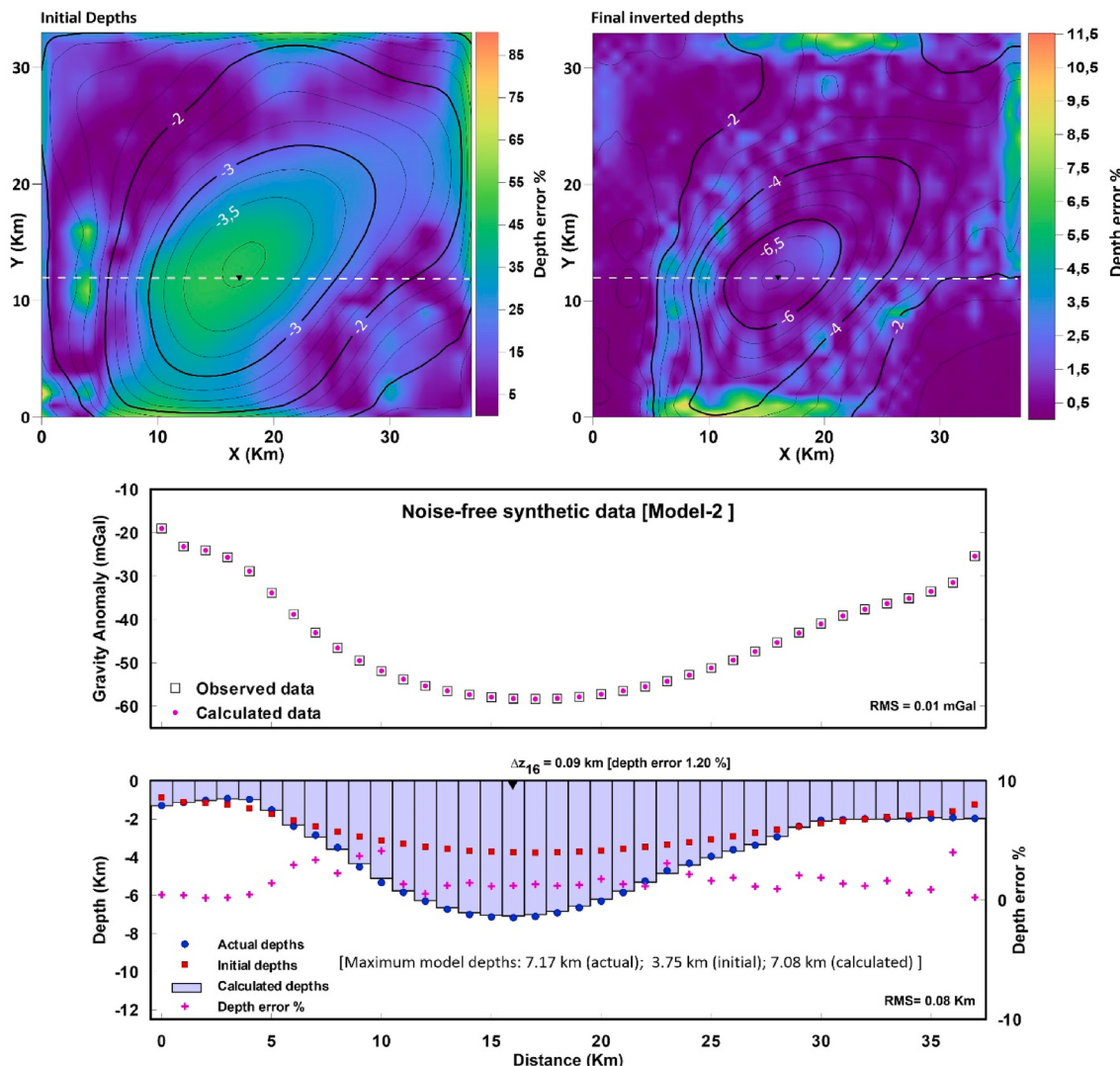


**Fig. 8.** Contour plots of the initial and the final inverted depths of the algorithm calculated from the noise-free synthetic data of Model-2 and their percentage errors according to the actual model depths (upper panel), and the results along a profile through the deepest point of the model in comparison with the actual data (lower panel). The white lines on the maps show the location of the profile data presented in the lower panel. The triangle symbol denotes the horizontal location of the deepest point of the actual depth model.

vertically and horizontally.

**Model-1:** Fig. 3a illustrates the view of a 3D simulated basin model as well as its plan view with a maximum depth of 5.2 km representing two basement depressions separated by a smooth basement high. The model is constructed through a  $60 \times 60$  mesh of horizontally juxtaposed rectangular prisms with lateral sizes of 1 km, their tops on the surface and thicknesses model the depths of the basement. The density model of the basin is considered to vary vertically and horizontally at the same time defined by the equation:  $\rho(x, y, z) = -0.6e^{-\lambda(xy)z}$  where the lateral variation of  $\lambda$  is in the range of 0.003–0.26  $\text{km}^{-1}$  as shown in Fig. 3b. Fig. 3c shows the theoretical gravity anomalies due to the simulated depth model obtained from application of the Chai and Hinze (1988) method (Eq. (4)). Using these data as the input in Grav3CH\_inv code and setting the greatest error  $\varphi$  for the stopping criteria within a threshold value of 0.1 mGal, forty-five iterations were performed by the inverse procedure described above for approximation of the calculated to the observed gravity anomalies. The depth estimates from the algorithm are shown in Fig. 4a, and the modeled gravity anomalies due to the inverted depths are shown in Fig. 4b. From the visual comparison of Figs. 4a and 3a, it is observed that the inverted depths compared well with the theoretical depths, and consequently, the gravity anomalies from the

inverted depths (Fig. 4b) were also compatible with the observed anomalies (Fig. 3c). Fig. 4c shows the difference between the model and the inverted basement depths. The RMS error between them was 0.0018 km. The residual between the real and the duplicated gravity anomalies was in the range of  $-0.04$  mGal to  $0.08$  mGal, where a major amount of these misfits was close to zero. The RMS after the initial stage was 10.83 mGal and reduced to 0.007 mGal at the stopping step (Fig. 4e), whereas the largest error  $\varphi$  fell down from 28.04 mGal to 0.09 mGal (Fig. 4f). The upper panel in Fig. 5 compares the percentage errors between the actual model depths of Model-1 and the initial and final model depths calculated from the algorithm. A profile view of the results along a line through the deepest point of the basin model is also illustrated in the lower panel of Fig. 5 in order to further present the fit between the actual and estimated depths. Here, the greatest depth error for both the initial and final models corresponds to the deepest point of the basin. The maximum depth of the actual basin model (5.2 km) was calculated as 12.02 km with 131 percent depth error in the initial stage, and 5.56 km with 6.9 percent depth error in the final inverted model. On the other hand, it can be seen that the initial depths are more compatible with the actual ones at the shallow depths of the model, and less at the deeper parts as expected. However, although the algorithm performs an equal

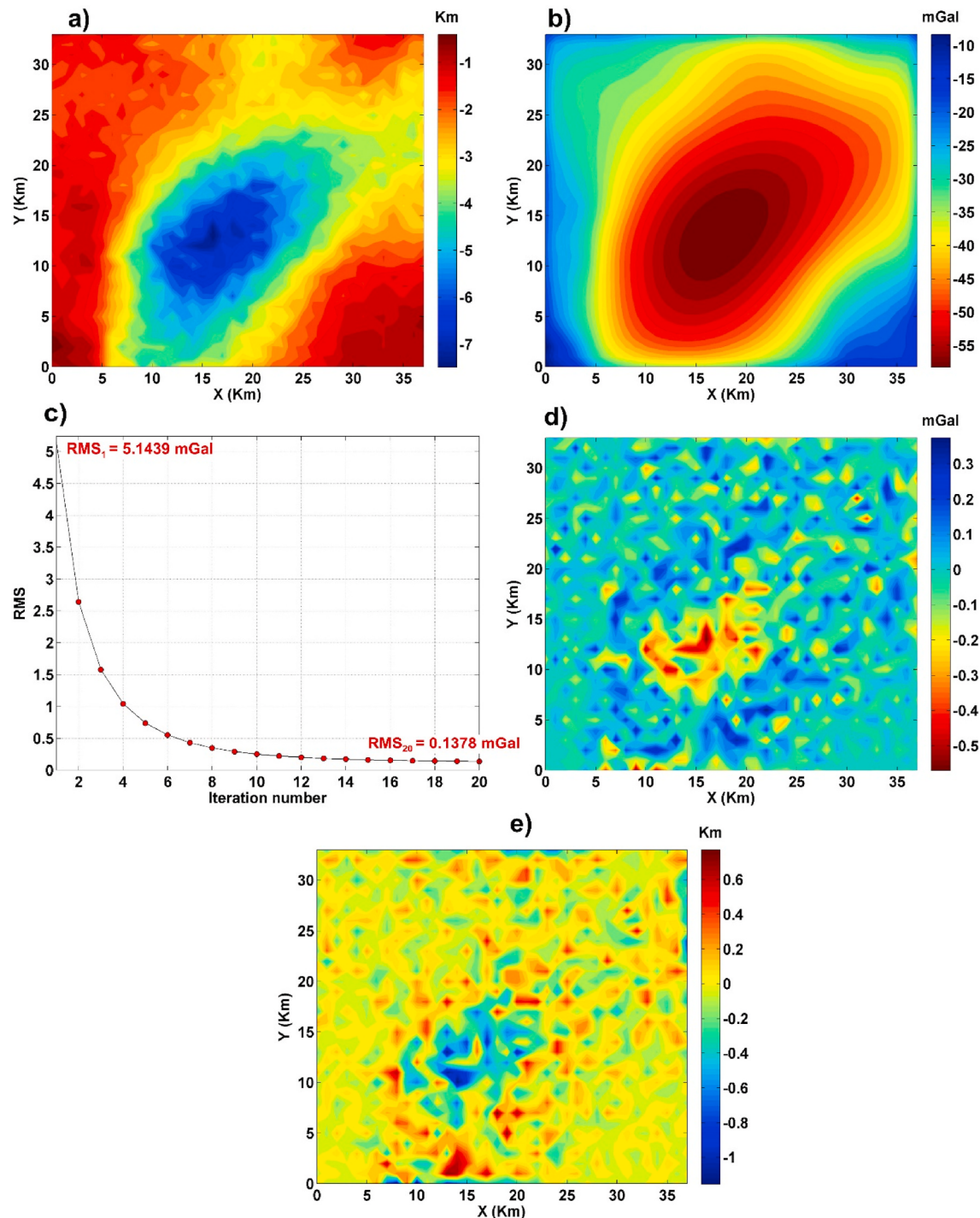


**Fig. 9.** Modelling results of Model-2 in case of 1% random noise included, (a) inverted depths, (b) calculated gravity anomaly from the inverted depth, (c) variation of RMS error versus iteration number, (d) the difference between observed and computed gravity anomaly, (e) the difference between the actual and inverted depths.

number of depth modifications for each the calculation point, it can be seen that the depth model recovered from the end of the procedure mimics the actual model well at all points along the profile. Also, considering the depth percentage errors of the final model, it is seen that the amount in depth error is generally less than 1 percent, except for the deepest part of the basin. Nevertheless, the depth error of 6.9 percent obtained for the deepest point of the basin that is also the highest along the profile can be accepted as reasonable considering the complex structure of the basin. The modelling of  $60 \times 60$  gridded data with a 1.8 GHz configured computer used only 1.5 s per iteration which was a short

duration for such an inverse problem.

**Model-2:** The second scenario of synthetic data application consisted of a deeper basin model up to 7.17 km with an elongated shape, and the sediment density contrast model was considered to vary only vertically defined by the exponential equation:  $\Delta\rho = -0.57e^{-0.25z}$ . In this case, the modelling procedure was also performed out through adding random noise to the model gravity anomaly in order to examine the efficacy of the proposed code on noise corrupted data. Fig. 6a illustrates the depth design of the basin constructed on  $38 \times 34$  mesh points with grid intervals of 1 km along the north and east directions. Fig. 6b shows

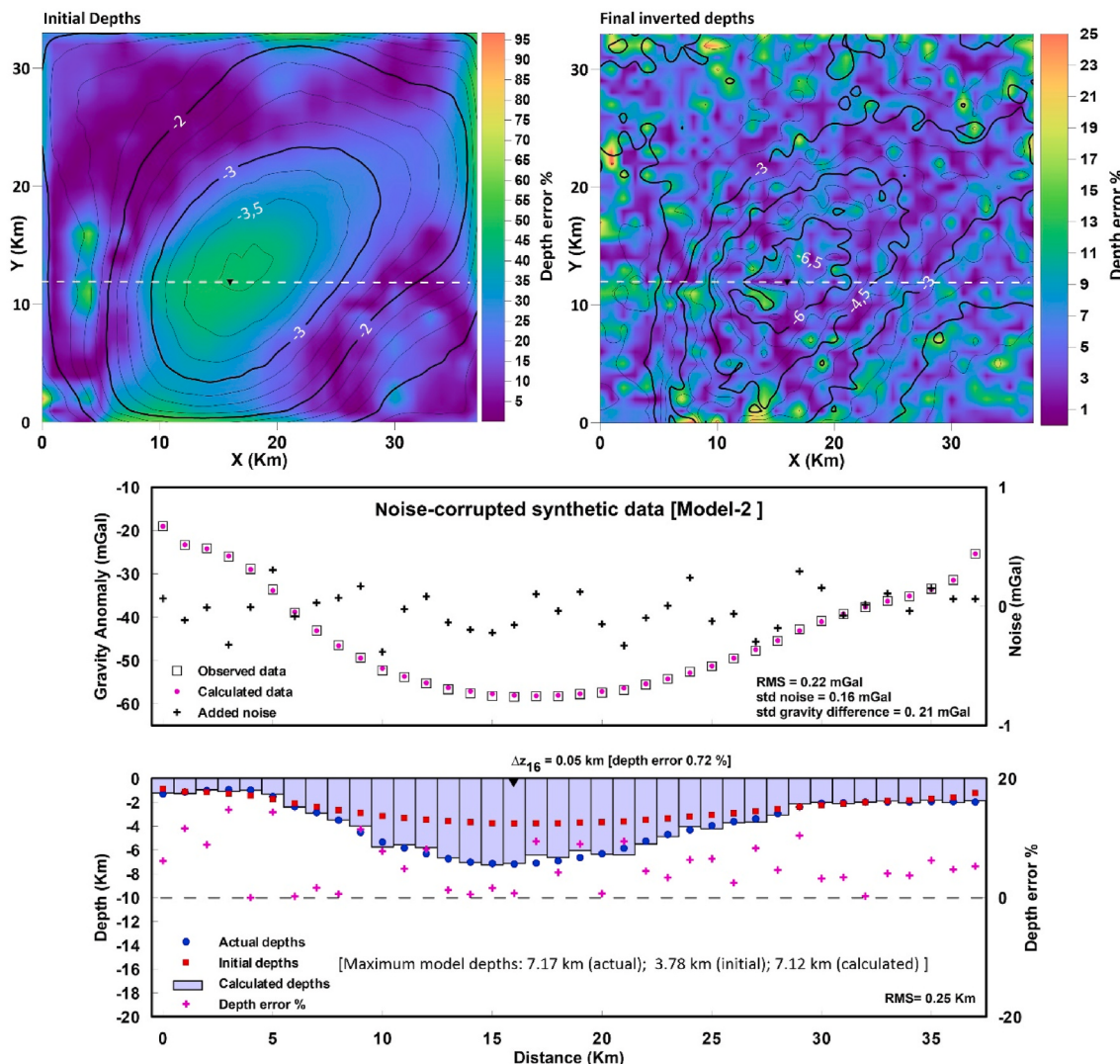


**Fig. 10.** Contour plots of the initial and the final inverted depths of the algorithm calculated from the noise-corrupted synthetic data of Model-2 and their percentage errors according to the actual model depths (upper panel), and the results along a profile through the deepest point of the model in comparison with the actual data (lower panel). The white lines on the maps show the location of the profile data presented in the lower panel. The triangle symbol denotes the horizontal location of the deepest point of the actual depth model.

the exponential curve of the density model, Fig. 6c is the noise-free synthetic gravity anomaly due to the model by Eq. (4), and Fig. 6d is the synthetic data contaminated with Gaussian noise with zero mean and 0.15 mGal standard deviation (std) obtained by

$$\Delta g_{obs\_noise} = \Delta g_{obs} + 0.15 \times randn(34, 38). \quad (9)$$

The inverted depths and the modeled gravity anomalies by the application of the Grav3CH\_inv code to the noise-free data of Model-2 are given in Fig. 7a and b, respectively. Hereby, the modelling scheme performed fifty-seven iterations, whereas the RMS at the initial stage between the modeled and the real gravity anomaly was 5.1428 mGal and fell down to the pre-assigned value of 0.01 mGal in the last iteration (Fig. 7c). Fig. 7d shows the residuals between the computed and actual gravity data which are in the range of  $\pm 0.03$  mGal, and the absolute depth differences between the actual and the re-constructed model were generally smaller than 0.2 km (Fig. 7e). The percentage errors between the actual model depths of Model-2 and the depths of the initial and the final models by the algorithm from the noise-free data is shown in the upper panel of Fig. 8. Here, the initial depths calculated by Eq. (5) are approximately 30 percent to 60 percent inaccurate compared to the actual depths around the main depression area of the basin model, but it

can be seen that these depth errors are mostly reduced to below 2 percent in the final model. The initial depth corresponding to the deepest point of the actual basin was calculated as 3.75 km. This is about 47.5 percent less than the actual value (7.17 km). At the end of the modelling procedure, the final inverted depth corresponding to this point resulted as 7.08 km that is about only 1.2 percent less from the actual depth (lower panel in Fig. 8). In addition, when the profile view of the results is examined, it can be seen that the calculated depths follow the actual basin model depths very closely along the profile. Here, the differences in depth between them were less than 0.1 km in general.

The modelling results from the noise-corrupted data of Model-2 are combined in Fig. 9. It can be seen that the inverted depths (Fig. 9a) were still compatible with those of the actual model given in Fig. 6a, where the residuals between them were in general smaller than 0.6 km (Fig. 9e) and at most of 1 km around the deeper parts of the basin. In this noisy case, the algorithm performed 20 iterations to duplicate the noise-corrupted gravity data with a maximum allowed misfit of  $\varphi = 0.5$  mGal. Fig. 9b shows the computed gravity anomalies, and Fig. 9d shows their residuals with the actual anomalies. The RMS error between them in the initial stage was 5.1439 mGal and was reduced to 0.1378 mGal in the final step (Fig. 9c). Fig. 10 show the maps of the initial and the final

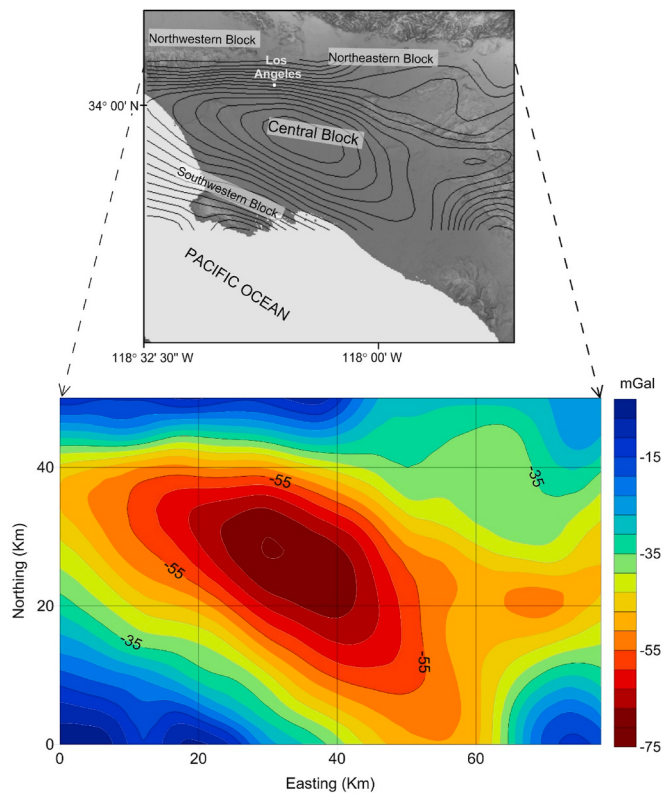


**Fig. 11.** Location map of the Los Angeles basin and the residual gravity anomalies over the basin digitized after Chai and Hinze (1988). Anomaly contours are drawn at 4 mGal interval.

inverted depth model by the algorithm from the noise-corrupted data of Model-2 and their percentage errors according to the actual model depths as well a profile view of the results through the deepest point of the basin model. The modelling procedure of the noise-corrupted data set produced a depth of 3.78 km for the maximum depth of the basin, with a depth error of 47.3 percent in the initial stage. The final inverted depth corresponding to this point at the end of the modelling procedure was 7.12 km which resulted in only 0.72 percent depth error from the actual depth (7.17 km). Also by comparing the results along the profile in the lower panel in Fig. 10, it can be seen that the depths calculated by the algorithm from the noisy data can still represent the real model with good agreement. Depths calculated here were generally obtained with depth errors of less than 5 percent in the deeper parts of the basin. Some depths calculated except for the deepest parts of the basin also show errors of up to 10 percent. However, these error amounts can be assumed still reasonable considering that the evaluated data are noisy. On the other hand, the std of the difference between the observed and calculated gravity anomalies of the whole area (Fig. 9d) was calculated to be 0.1376 mGal at a value slightly lower than the std of the added noise

**Table 1**

Comparison of the obtained maximum depths to the basement relief in Los Angeles basin.

| Source                              | Data and method                                 | Maximum depth to basement (km) |            |
|-------------------------------------|---|--------------------------------|------------|
| Chai and Hinze (1988)               | Gravity Data                                    | Forward Modelling              | 10         |
| McCulloh (1960)                     | Surface geology, Drill-hole, Seismic Reflection |                                | 9.5        |
| Bhaskara Rao and Ramesh Babu (1991) | Gravity   | Forward Modelling              | 9.5        |
| Malesh et al. (2019)                | Gravity   | Forward Modelling              | 9.73       |
| <b>Present study</b>                | Gravity   | Forward Modelling              | <b>9.7</b> |

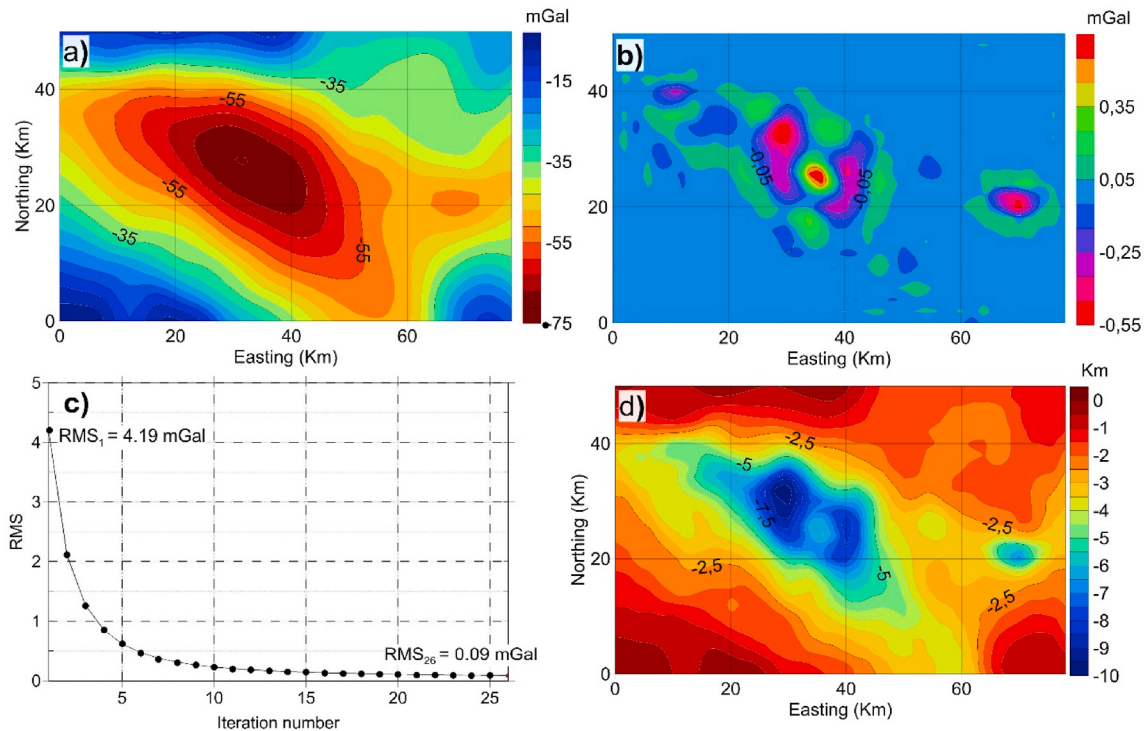


**Fig. 12.** (a) recalculated gravity anomaly based on the estimated depth to basement after twenty-six iterations (contour interval 4 mGal), (b) residuals between observed gravity (Fig. 11) and the recalculated gravity (Fig. 12a) drawn at 0.1 mGal contour interval, (c) plot of RMS error versus iteration number obtained during the iterative procedure, (d) basement surface of the basin obtained by the present algorithm (contour interval 0.5 km). Los Angeles basin, California.

content. This also indicates that the algorithm can be effective even in the presence of noise in the data.

## 5. Real field practice

The functional applicability of the Grav3CH\_inv code on real field data was tested by the example of the Los Angeles basin, previously analyzed also by several other researchers for its basement relief. The basin is known for its complex geology as well as its hydrocarbon potential. The development of the basin took place at five different phases, each representing its own distinct rock assemble (Yerkes et al., 1965). By this, the basin is differentiated into four main zones identified as southwest, northwest, central and northeast blocks (Fig. 11a) where each is bounded by a main fault zone or a folding in the underlying rocks (Yerkes et al., 1965). Among them, the main characteristic of the central block is the existence of a northwest-trending synclinal trough involving thick-layered sediments. Fig. 11b shows the gravity anomaly of the basin digitized after Chai and Hinze (1988) on a  $26 \times 40$  mesh point with 2 km intervals along the north and east directions, respectively. Here, the gravity anomaly pattern with high negative values over the central part reflect the structural expectation of the central block well. Based on the sample density data from McCulloh (1960), Chai and Hinze (1988) used an exponential density function defined by  $\Delta\rho = -0.5e^{-0.1609z}$  in their modelling strategy in order to obtain accurate depth estimates of the basin. Using the gravity data and the described density model as the inputs in the present code, the algorithm performed 26 iterations to duplicate the observed gravities with a maximum allowed misfit of RMS of 0.1 mGal. Fig. 12a illustrates the modeled gravity anomalies, and Fig. 12b shows the difference between the modeled and observed anomaly resulted with a mean absolute deviation of 0.044 mGal. The RMS after the initial stage was 4.19 mGal and was reduced to 0.09 mGal in the final step (Fig. 12c). The depth estimates (Fig. 12d) closely resembled those of the previously obtained by Chai and Hinze (1988), Bhaskara Rao and Ramesh Babu (1991) and Mallesh et al. (2019). On the other hand, the structure map by McCulloh (1960) based on seismic data and drill hole information revealed a value of 9.5 km for the deepest section of the basin. The maximum depth by Chai and Hinze (1988) to the basin floor was 10 km. Although the inverted interface geometry was comparable to that obtained by Chai and Hinze (1988), the highest sediment thickness from the present code was 9.7 km, which was also consistent with the results by Bhaskara Rao and Ramesh Babu (1991) and Mallesh et al. (2019) (Table 1). In contrast to the model by Chai and Hinze (1988), Mallesh et al. (2019) reported that the basin extends further south beyond the limits of the grid, being in accordance with the structural configuration of Yerkes et al. (1965). The present interpreted model also revealed such an extension to the south which was consistent with those of Mallesh et al. (2019) and Bhaskara Rao and Ramesh Babu (1991). Besides, the structure calculated from the present interpretation brought out a basement high separating two depressions in the north-south trend (Fig. 12d) which were also reflected prominently in the model of Mallesh et al. (2019).

## 6. Conclusion

This study deals with a GUI-based MATLAB program, Grav3CH\_inv, performing 3D modelling of gravity anomalies over a sedimentary basin to estimate its basement relief. The algorithm linked to the developed code enhances the accuracy of computations by incorporating the exponential depth relation function for the increase in density with depth where it can be set as well to vary laterally to consider also the horizontal density variations of the model space. The procedure starts with an initial depth model of the basement structure obtained by substituting the observed gravity anomalies, as well as the density model in the inverted Bouguer slab relation, and iteratively improves the depth estimates until a desired match between the actual and calculated gravity anomalies is achieved. Hereby, the precision in computing

model gravity anomalies due to temporal depth estimates in the ongoing process is increased by using the shift sampling technique of computing the numerical inverse Fourier transform. As a further advantage, the operational flow chart of the algorithm does not necessitate an average depth plane of the interface or filtering of data during or prior to processing. The GUI-supported interactive control functions of the Grav3CH\_inv code allow users to set optional settings, display the style of outputs and export formats, and they do not require coding expertise to perform the relevant procedures of the algorithm.

In order to demonstrate the practical application and reliability of the present code, three cases, two synthetically produced sets of data from different configurations of depth and density models where one also includes random noise and an actual dataset are presented. The depth results calculated from both noise-free data samples matched the actual depth models well. Although there were some minor deviations between the actual and estimated depths from the noise-corrupted data example, the results on the whole were also in good agreement considering the fact that the given gravity anomalies that were operated were noisy. The code was applied for real the field example by re-analyzing the gravity dataset of the Los Angeles Basin, which has been interpreted previously also by other researchers for its basement relief. The approximated depth structure of the basin after an optimal correlation between the real and calculated gravity anomalies resulted in a close agreement with the previously reported ones. As a result, the proposed code proved to be effective in interpreting gravitational anomalies to determine the basement surface of sedimentary basins, and hence, it may therefore be considered as a practical tool for basin modelling purposes in geophysical applications.

## Availability of the code

The Grav3CH\_inv.m code is in free access and open in source program with 44 KB in size available at [https://github.com/OksumE/Grav3CH\\_inv](https://github.com/OksumE/Grav3CH_inv). The code can be executed in any hardware in which the R2013b or a higher version of MATLAB software is installed.

## Declaration of competing interest

The authors declare that they have no known competing financial interests or personal relationships that could have appeared to influence the work reported in this paper.

## Acknowledgements

The author record with pleasure his sincere thanks to the anonymous reviewers and Editor Dario Grana for their very constructive suggestions to improve the manuscript.

## Appendix A. Supplementary data

Supplementary data to this article can be found online at <https://doi.org/10.1016/j.cageo.2021.104856>.

## References

- Athy, L.F., 1930. Density, porosity and compaction of sedimentary rocks. Bull. Am. Assoc. Pet. Geol. 14, 1–24.
- Barbosa, V.C.F., Silva, J.B.C., Medeiros, W.E., 1997. Gravity inversion of basement relief using approximate equality constraints on depths. Geophysics 62 (6), 1745–1757.
- Barbosa, V.C.F., Silva, J.B.C., Medeiros, W.E., 1999. Gravity inversion of a discontinuous relief stabilized by weighted smoothness constraints on depth. Geophysics 64 (5), 1429–1437.
- Bhaskara Rao, D., 1986. Modeling of sedimentary basins from gravity anomalies with variable density contrast. Geophys. J. Int. 84, 207–212.
- Bhaskara Rao, D., Ramesh Babu, N., 1991. A Fortran-77 computer program for three-dimensional analysis of gravity anomalies with variable density contrast. Comput. Geosci. 17 (5), 655–667.

- Bhaskara Rao, D., Prakash, M.J., Ramesh Babu, N., 1993. Gravity interpretation using Fourier transforms and simple geometrical models with exponential density contrast. *Geophysics* 58, 1074–1083.
- Bohidar, R.N., Sullivan, J.P., Hermance, J.F., 2001. Delineating depth to bedrock beneath shallow unconfined aquifers: a gravity transect across the Palmer River Basin. *Ground Water* 39 (5), 729–736.
- Bott, M.H.P., 1960. The use of rapid digital computing methods for direct gravity interpretation of sedimentary basins. *Geophys. J. Roy. Astron. Soc.* 3, 63–67.
- Cai, H., Zhdanov, M., 2015. Application of Cauchy-type integrals in developing effective methods for depth-to-basement inversion of gravity and gravity gradiometry data. *Geophysics* 80 (2), G81–G94. <https://doi.org/10.1190/geo2014-0332.1>.
- Chai, Y., Hinze, W.J., 1988. Gravity inversion of an interface above which the density contrast varies exponentially with depth. *Geophysics* 53, 837–845.
- Chakravarthi, V., 2009. Automatic gravity inversion for simultaneous estimation of model parameters and regional gravity background: an application to 2D pull-apart basins. *Curr. Sci.* 96 (10), 1349–1360.
- Chakravarthi, V., Raghuram, H.M., Singh, S.B., 2002. 3D Forward gravity modeling of density interfaces above which the density contrast varies continuously with depth. *Comput. Geosci.* 28, 53–57.
- Chakravarthi, V., Sundararajan, N., 2004. Automatic 3-D gravity modeling of sedimentary basins with density contrast varying parabolically with depth. *Comput. Geosci.* 30, 601–607.
- Chakravarthi, V., Shankar, G.B.K., Muralidharan, D., Harinarayana, T., Sundararajan, N., 2007. An integrated geophysical approach for imaging subbasalt sedimentary basins: case study of Jam River Basin, India. *Geophysics* 72, B141–B147.
- Chakravarthi, V., Sastry, S.R., Ramamma, B., 2013. MODTOHAFSD—a GUI based JAVA code for gravity analysis of strike limited sedimentary basins by means of growing bodies with exponential density contrast-depth variation: a space domain approach. *Comput. Geosci.* 56, 131–141.
- Chakravarthi, V., Ramamma, B., 2015. Determination of sedimentary basin basement depth: a space domain based gravity inversion using exponential density function. *Acta Geophys.* 63 (4), 1066–1079.
- Chakravarthi, V., Mallesh, K., Ramamma, B., 2017. Basement depth estimation from gravity anomalies: two 2.5D approaches coupled with the exponential density contrast model. *J. Geophys. Eng.* 14 (2), 303–315.
- Chappell, A., Kusznir, N., 2008. An algorithm to calculate the gravity anomaly of sedimentary basins with exponential density-depth relationships. *Geophys. Prospect.* 56, 249–258.
- Cordell, L., Henderson, R.G., 1968. Iterative three-dimensional solution of gravity anomaly data using a digital computer. *Geophysics* 33, 596–601.
- Cordell, L., 1973. Gravity anomalies using an exponential density-depth function - san Jacinto Graben, California. *Geophysics* 38, 684–690.
- Crosby, A.G., McKenzie, D., Slater, J.G., 2006. The relationship between depth, age and gravity in the oceans. *Geophys. J. Int.* 166 (2), 553–573.
- Ekinci, Y.L., Balkaya, C., Gokturkler, G., Ozyalin, S., 2021. Gravity data inversion for the basement relief delineation through global optimization: a case study from the Aegean Graben System, western Anatolia, Turkey. *Geophys. J. Int.* 224 (2), 923–944.
- Feng, J., Zhang, S., Meng, X., 2016. Constraint 3D density interface inversion from gravity anomalies. *Arabian Journal of Geoscience* 9 (1). <https://doi.org/10.1007/s12517-015-2213-9>.
- Feng, J., Meng, X., Chen, Z., Zhang, S., 2014. Three-dimensional density interface inversion of gravity anomalies in the spectral domain. *J. Geophys. Eng.* 11, 035001. <https://doi.org/10.1088/1742-2132/11/3/035001>.
- Florio, G., 2020. The estimation of depth to basement under sedimentary basins from gravity data: review of approaches and the ITRESC method, with an application to the Yucca Flat Basin (Nevada). *Surv. Geophys.* 41, 935–961.
- Garcia-Abdeslem, J., 1992. Gravitational attraction of a rectangular prism with depth-dependent density. *Geophysics* 57 (3), 470–473.
- Garcia-Abdeslem, J., 2005. The gravitational attraction of a right rectangular prism with density varying with depth following a cubic polynomial. *Geophysics* 70 (6), J39–J42.
- Gomez-Ortiz, D., Agarwal, B.N.P., 2005. 3DINVER.M: a MATLAB program to invert gravity anomaly over a 3-D horizontal density interface by Parker-Oldenburg's algorithm. *Comput. Geosci.* 31, 513–520.
- Granser, H., 1987. Three - dimensional interpretation of gravity data from sedimentary basins using an exponential density – depth function. *Geophys. Prospect.* 35, 1030–1041.
- Gu, X., Tenzer, R., Gladkikh, V., 2014. Empirical models of the ocean-sediment and marine sediment-bedrock density contrasts. *Geosci. J.* 18, 439–447.
- Hedberg, H.D., 1936. The gravitational compaction of clays and shales. *Am. J. Sci.* 31, 241–287.
- Himi, M., Tapias, J., Benabdoulahab, S., Salhi, A., Rivero, L., Elgettafi, M., El Mandour, A., Stitou, J., Casas, A., 2017. Geophysical characterization of saltwater intrusion in a coastal aquifer: the case of Martil-Alila plain (North Morocco). *J. Afr. Earth Sci.* 126, 136–147.
- Hughes, D.S., Cooke Jr., C.E., 1953. The effect of pressure on the reduction of pore volume of consolidated sandstones. *Geophysics* 18, 298–309.
- Lekula, M., Lubczynski, M.W., Shemang, E.M., 2018. Hydrogeological conceptual model of large and complex sedimentary aquifer systems—central Kalahari Basin (Botswana). *Phys. Chem. Earth* 106, 47–62.
- Litinsky, V.A., 1989. Concept of effective density: key to gravity depth de-terminations for sedimentary basins. *Geophysics* 54, 1474–1482.
- Mallesh, K., Chakravarthi, V., Ramamma, B., 2019. 3D gravity analysis in the spatial domain: model simulation by multiple polygonal cross-sections coupled with exponential density contrast. *Pure Appl. Geophys.* 176, 2497–2511.
- Mantlik, F., Matias, M., Lourenco, J., Grangeia, C., Tareco, H., 2009. The use of gravity methods in the internal characterization of landfills—a case study. *J. Geophys. Eng.* 6, 357–364.
- Maxant, J., 1980. Variation of density with rock type, depth, and formation in the Western Canada basin from density logs. *Geophysics* 45 (6), 1061–1076.
- McCulloh, J.H., 1960. Gravity Variation and the Geology of the Los Angeles Basin of California. U.S.G.S. Prof. Paper 400B. B320–B325.
- Mendonca, C.A., 2004. Inversion of gravity field inclination to map the basement relief of sedimentary basins. *Geophysics* 69, 1240–1251.
- Murthy, I.V.R., Rao, D.B., 1979. Gravity anomalies of two dimensional bodies of irregular cross section with density contrast varying with depth. *Geophysics* 44, 1525–1530.
- Murthy, I.V.R., Rao, S.J., 1989. A Fortran 77 program for inverting gravity anomalies of two-dimensional basement structures. *Comput. Geosci.* 15, 1149–1156.
- Nagendra, R., Prasad, P.V.S., Bhimasankaram, V.L.S., 1996. Forward and inverse computer modeling of gravity field resulting from a density interface using Parker-Oldenburg method. *Comput. Geosci.* 22, 227–231.
- Oldenburg, D.W., 1974. The inversion and interpretation of gravity anomalies. *Geophysics* 39 (4), 526–536.
- Pallero, J.L.G., Fernandez-Martinez, J.L., Bonvalot, S., Fudym, O., 2015. Gravity inversion and uncertainty assessment of basement relief via particle swarm optimization. *J. Appl. Geophys.* 116, 180–191.
- Pallero, J.L.G., Fernandez-Martinez, J.L., Bonvalot, S., Fudym, O., 2017. 3D gravity inversion and uncertainty assessment of basement relief via particle swarm optimization. *J. Appl. Geophys.* 139, 338–350.
- Parker, R.L., 1973. The rapid calculation of potential anomalies. *Geophys. J. Int.* 31, 447–455.
- Pham, L.T., Oksum, E., Do, T.D., 2018. GCH.gravinv: a MATLAB-based program for inverting gravity anomalies over sedimentary basins. *Comput. Geosci.* 120, 40–47.
- Silva, J.B.C., Costa, D.C.L., Barbosa, V.C.F., 2006. Gravity inversion of basement relief and estimation of density contrast variation with depth. *Geophysics* 71 (5), J51–J58.
- Silva, J.B.C., Oliveira, A.S., Barbosa, V.C.F., 2010. Gravity inversion of 2D basement relief using entropic regularization. *Geophysics* 75, I29–I35.
- Silva, J.B.C., Santos, D.F., 2017. Efficient gravity inversion of basement relief using a versatile modeling algorithm. *Geophysics* 82, 23–34.
- Shin, Y.H., Choi, K.S., Xu, H., 2006. Three-dimensional forward and inverse models for gravity fields based on the Fast Fourier Transform. *Comput. Geosci.* 32, 727–738.
- Talwani, M., Worzel, J., Ladisman, M., 1959. Rapid gravity computations for two dimensional bodies with application to the Mendocino submarine fracture zone. *J. Geophys. Res.* 64, 49–59.
- Tenzer, R., Gladkikh, V., 2014. Assessment of density variations of marine sediments with ocean and sediment depths. *Sci. World J.* 823296, 1–9, 2014.
- Venteris, E., Miller, M., 1993. Gravitational Profiles on the Taku Glacier System. Glaciological and Arctic Sciences Institute, University of Idaho, Open File Report.
- Yerkes, R.F., McCulloh, T.H., Schoellhamer, J.E., Vedder, J.G., 1965. Geology of the Eastern Los Angeles Basin, California—an Introduction. Geological Survey Professional Paper 420-A. United States Government Printing Office <https://pubs.usgs.gov/pp/0420a/report.pdf>. Accessed. (Accessed 8 August 2019).